First coordination compounds based on a bis(imino nitroxide) biradical and 4f metal ions: Synthesis, crystal structures and

Dalton Transactions

PAPER

View Article Online
View Journal | View Issue

Cite this: *Dalton Trans.*, 2016, **45**, 2936

First coordination compounds based on a bis-(imino nitroxide) biradical and 4f metal ions: synthesis, crystal structures and magnetic properties†

Samira G. Reis,[a] Matteo Briganti,[b] Daniel O. T. A. Martins,[a] Handan Akpinar,[c] Sergiu Calancea,[a] Guilherme P. Guedes,[d] Stéphane Soriano,[e] Marius Andruh,[f] Rafael A. A. Cassaro,[g] Paul M. Lahti,*[c] Federico Totti[b] and Maria G. F. Vaz*[a]

Received 12th November 2015,
Accepted 22nd December 2015

DOI: 10.1039/c5dt04469c

www.rsc.org/dalton

The synthesis, crystal structures and magnetic properties of two families of heterospin complexes containing lanthanide ions and a bis(imino nitroxide) biradical (IPhIN = 1-iodo-3,5-bis(4′,4′,5′,5′-tetramethyl-4′,5′-dihydro-1*H*-imidazole-1′-oxyl)benzene) are reported: in $[Ln_2(hfac)_6(IPhIN)(H_2O)_2]$ compounds, two lanthanide ions [Ln = Gd^{III} (**1**) and Dy^{III} (**2**)] are coordinated to the biradical, and in $[Ln(hfac)_3(IPhIN)(H_2O)]$ compounds, one lanthanide ion (Ln = Tb^{III} (**3**), Gd^{III} (**4**) or Dy^{III} (**5**)) is coordinated to the biradical. Ferromagnetic intramolecular magnetic interactions between Gd^{III} and the biradical were found for **1** and **4**, while intramolecular magnetic interactions between the radicals were ferro- and antiferromagnetic, respectively. Compound **2** shows a field induced slow relaxation of magnetization, which (under an external applied field of 2 kOe) exhibits an activation energy barrier of $\Delta E/k_B$ = 27 K and a pre-exponential factor of 1.4×10^{-8} s. To support the magnetic characterization of compound **3** *ab initio* calculations were also performed.

1 Introduction

The use of stable organic radicals as building blocks is a well-established strategy towards designing new molecular magnetic compounds,[1] and a new burst of interest arose after the discovery of single chain magnet behavior in a heterospin system containing an organic radical coordinated to a metal ion.[2,3] Although much effort has been made using the nitronyl nitroxide and nitroxide (aminoxyl) monoradical units, the use of organic biradicals is relatively less explored. The latter are very appealing because the intramolecular magnetic exchange interactions between two radical moieties can be designed and widely tuned within the same biradical unit by choosing an appropriate conjugated spacer to link the radical spins. This allows wider control of the magnetic properties of a metal–radical system than can be achieved using simpler monoradicals.

Recently, some of us reported metal–radical systems containing a bis(imino nitroxide) biradical.[4] The major reason for exploring the use of this biradical is that it has four coordination sites: two oxygens and two azole nitrogen donors from nitroxide and imidazole moieties, respectively. These distinguishable coordinating sites can give rise to a large variety of heterospin complexes. Among the possibilities, lanthanide ions are particularly good choices for coordination compounds, because of their large uniaxial magnetic anisotropy and large magnetic moments that could exhibit magnetic hysteresis due to slow relaxation of the magnetization. This magnetic behavior is observed in single molecule magnets (SMMs), single chain magnets (SCMs) and more recently single ion magnets (SIMs).[2,5] These types of compounds are being intensively studied due to their potential application in

[a]*Instituto de Química, Universidade Federal Fluminense, Niterói 24020-150, RJ, Brazil. E-mail: mariavaz@vm.uff.br*
[b]*Dipartimento di Chimica, Università degli Studi di Firenze, 50019 Sesto Fiorentino, Firenze, Italy*
[c]*Department of Chemistry, University of Massachusetts, Amherst, Massachusetts, 01003 USA. E-mail: lahti@chem.umass.edu*
[d]*Instituto de Ciências Exatas, Departamento de Química, Universidade Federal Rural do Rio de Janeiro, Seropédica 23851-970, RJ, Brazil*
[e]*Instituto de Física, Universidade Federal Fluminense, Niterói 24210-346, RJ, Brazil*
[f]*Inorganic Chemistry Laboratory, Faculty of Chemistry, University of Bucharest, Str. Dumbrava Rosie nr. 23, 020464-Bucharest, Romania*
[g]*Instituto de Química, Universidade Federal do Rio de Janeiro, Rio de Janeiro 21941-909, RJ, Brazil*

†Electronic supplementary information (ESI) available: Geometry parameters associated with hydrogen bonding for compounds **1–3** are listed in Table S1. A summary of crystal structure, data collection and refinement for **4** is compiled in Table S2. Fig. S1 and S2 show powder XRD for **1**, **2** and **4**, **5**. Fig. S3–S5 show the field dependence of the magnetization for compounds **2**, **3** and **5**. Ac magnetic data, Arrhenius and Cole–Cole plots for **2** are shown in Fig. S6–S8. CCDC 1404060–1404062 and 1424570 for **1–3** and **5** respectively. For ESI and crystallographic data in CIF or other electronic format see DOI: 10.1039/c5dt04469c

high-density data storage materials and quantum computations, as well as to understand their unusual magnetic quantum behaviors.[6] Much effort has been expended to increase the blocking temperatures of slow relaxing magnetic systems,[7] and lanthanide-based coordination compounds are very promising due to their large magnetic anisotropy.[8] Some coordination compounds containing organic bis(nitronyl nitroxide) ligands exhibiting slow magnetic relaxation have been reported.[9–11] However, to our knowledge there are no reported examples of lanthanide-based coordination compounds with bis(imino nitroxide) ligands. Therefore, we focused on the coordination of block-f metal ions using the bis(imino nitroxide) biradical previously used by some of us – 1-iodo-3,5-bis-(4′,4′,5′,5′-tetramethyl-4′,5′-dihydro-1*H*-imidazole-1′-oxyl)benzene (IPhIN) – for coordination with non-lanthanide metals.[4] Herein, we report the synthesis, crystal structures and magnetic properties of two families of heterospin complexes containing lanthanide ions and the IPhIN biradical. The first family consists of dinuclear units with the general formula $[Ln_2(hfac)_6(IPhIN)(H_2O)_2]$ (Ln = Gd^{III} (**1**) and Dy^{III} (**2**)), in which the metal ions are bridged by the IPhIN. In the second one, the IPhIN radical is monocoordinated to $\{Ln(hfac)_3\}$ units leading to mononuclear species $[Ln(hfac)_3(IPhIN)(H_2O)]$ (Ln = Tb^{III} (**3**), Gd^{III} (**4**) or Dy^{III} (**5**)). The magnetic properties were investigated and the data were analysed using models that consider two exchange couplings in order to take into account the metal–radical and radical–radical (intramolecular) magnetic exchange. CASSCF/RASSI-SO *ab initio* calculations were performed to support the magnetic interpretation. Compound **2** displays slow relaxation of its magnetization.

2 Experimental section

2.1 General procedures

All reagents and solvents were purchased from commercial sources and used without additional purification. The $[Ln(hfac)_3]$ (Ln = Gd^{III}, Dy^{III} and Tb^{III}) and IPhIN building blocks were synthesized as described elsewhere.[4,12]

2.2 Synthesis of complexes 1–5

A suspension containing 0.12 mmol of an appropriate $[Ln(hfac)_3]$ hydrate (Ln = Gd^{III} (**1** and **4**), Dy^{III} (**2** and **5**) or Tb^{III} (**3**)) in 20 mL of *n*-heptane was boiled until dissolution. Then, 0.021 g (0.06 mmol) of IPhIN dissolved in 2 mL of $CHCl_3$ was added with stirring. The solution was kept at 10 °C, and after 10 days pale pink prism (**1–2**) or dark violet block (**3–5**) crystals were obtained. Single crystals were manually separated from the mother liquor to maintain maximum purity: these were washed with *n*-heptane, and dried in air. For $[Ln(hfac)_3{\cdot}nH_2O]$ where Ln = Gd and Dy, two types of crystals were always observed in the final product, even when the reactant stoichiometry was varied. Powder X-ray diffraction patterns for **1**, **2**, **4** and **5** were compared with the simulated powder diffraction pattern predicted from the crystal structure. The experimental and simulated peaks corresponded well in position and relative intensity, confirming the phase purity of the compounds separated manually (see the ESI for details, Fig. S1 and S2†).

Compound (**1**): analysis calculated for $C_{50}H_{37}F_{36}Gd_2IN_4O_{16}$ C 28.94, H 1.80, N 2.70; found C 29.05, H 2.15, N 2.56; IR (ATR, ν cm^{-1}): 3353 (b, O–H), 3197 (w, C–H aromatic), 2996, 2962 (w, C–H aliphatic), 1647 (s, C═O), 1252, 1194, 1133 (s, C–F).

Compound (**2**): analysis calc. for $C_{50}H_{37}F_{36}Dy_2IN_4O_{16}$ C 28.79, H 1.80, N 2.69; found C 28.62, H 2.07, N 2.99; IR: 3343 (b, O–H), 3050 (w, C–H aromatic), 2960, 2920 (w, C–H-aliphatic), 1651 (s, C═O), 1249, 1191, 1136 (s, C–F).

Compound (**3**): analysis calc. for $C_{35}H_{32}F_{18}IN_4O_9Tb$ C 32.83, H 2.52, N 4.38; found C 32.56, H 2.37, N 4.51; IR: 3341 (b, O–H), 3082 (w, C–H aromatic), 2989, 2932 (w, C–H aliphatic), 1654 (s, C═O), 1251, 1194, 1137 (s, C–F).

Compound (**4**): analysis calc. for $C_{35}H_{32}F_{18}IN_4O_9Gd$ C 32.83, H 2.52, N 4.38; found C 33.10, H 2.98, N 4.35; IR: 3341 (b, O–H), 3147 (w, C–H aromatic), 2979 (w, C–H aliphatic), 1649 (s, C═O), 1252, 1194, 1134 (s, C–F).

Compound (**5**): analysis calc. for $C_{35}H_{32}F_{18}IN_4O_9Dy$ C 32.74, H 2.51, N 4.36; found C 32.77, H 2.62, N 4.27; IR: 3427 (w, O–H), 3146 (w, C–H aromatic), 2980 (w, C–H aliphatic), 1649 (s, C═O), 1252, 1194, 1135 (s, C–F).

2.3 X-ray diffraction

Powder X-ray diffraction data for all the samples were collected on a Bruker D8 Advance equipped with a LynxEye detector. Single crystal X-ray data were collected on an Oxford GEMINI A Ultra diffractometer for **1–3** at 120 K and on a Bruker D8 Venture diffractometer for **4–5** at 150 K and 293 K, respectively, using graphite monochromated Mo Kα radiation (λ = 0.71073 Å). Data collection, data reduction, cell refinement and absorption corrections for **1–3** were performed using the CrysAlis RED software, Oxford Diffraction Ltd, Version 1.171.32.38. For **4–5**, data collection and cell refinement were performed using Bruker Instrument Service v4.2.2 software and APEX2,[13] respectively. Data reduction was carried out using SAINT.[14] Empirical multiscan absorption correction using equivalent reflections was performed using the SADABS program.[15] The crystal structures were solved using SHELXS-97 software, and structure refinement was performed using SHELXL-97 software based on F^2 through full-matrix least squares routines.[16] All atoms except hydrogen were refined anisotropically. The H-atoms were treated by a mixture of independent and constrained refinement. Crystals of **4** had limited quality and the crystal structure could not be refined well (see the ESI† for details). Details of data collection and structure refinement for compounds **1–3** and **5** are summarized in Table 1. Selected bond lengths and angles are given in Table 2.

2.4 Magnetic measurements

Dc magnetic measurements were carried out using a Cryogenic SX600 SQUID magnetometer for compounds **1–4** and a Quantum Design MPMS XL-7 SQUID magnetometer for compound **5**. Freshly prepared single crystals were placed in a

Table 1 Summary of crystal data collection and refinement parameters for compounds 1–3 and 5

Compound reference	(1)	(2)	(3)	(5)
Chemical formula	$C_{50}H_{37}F_{36}Gd_2IN_4O_{16}$	$C_{50}H_{37}F_{36}Dy_2IN_4O_{16}$	$C_{35}H_{32}F_{18}IN_4O_9Tb$	$C_{35}H_{32}F_{18}IN_4O_9Dy$
Formula mass	2075.24	2085.74	1280.48	1284.05
Crystal system	Triclinic	Triclinic	Monoclinic	Monoclinic
a/Å	12.5796(6)	12.5244(8)	15.2202(4)	15.2921(9)
b/Å	13.3674(5)	13.2968(9)	12.2385(3)	12.4066(8)
c/Å	23.2909(13)	23.3803(16)	25.4334(7)	26.1003(17)
α/°	89.610(4)	89.620(6)	90	90
β/°	83.439(4)	83.290(6)	99.026(3)	99.137(2)
γ/°	64.895(4)	65.009(7)	90	90
Unit cell volume/Å^3	3519.5(3)	3501.0(5)	4678.9(2)	4889.0(5)
Temperature/K	120	120	120	293
Space group	$P\bar{1}$	$P\bar{1}$	$P2_1/c$	$P2_1/c$
Z	2	2	4	4
Radiation type	MoKα	MoKα	MoKα	MoKα
μ/mm^{-1}	2.47	2.72	2.30	2.28
Reflections measured	27 378	17 967	31 832	42 345
Independent reflections	12 415	12 352	8273	8653
R_{int}	0.051	0.076	0.042	0.031
R_1 values ($I > 2\sigma(I)$)	0.055	0.082	0.05	0.124
w$R(F^2)$ values ($I > 2\sigma(I)$)	0.126	0.208	0.120	0.279
R_1 values (all data)	0.081	0.129	0.063	0.135
w$R(F^2)$ values (all data)	0.146	0.260	0.128	0.272
Goodness of fit on F^2	1.03	1.03	1.04	1.07
CCDC deposition	1404060	1404061	1404062	1424570

Table 2 Selected bond lengths (Å) and bond angles (°) for compounds 1–3 and 5

Atom labels	(1) (Ln = Gd)	(2) (Ln = Dy)	(3) (Ln = Tb)	(5) (Ln = Dy)
Ln1–O1	2.379(5)	2.331(9)	2.275(4)	2.270(9)
Ln1–O2	2.385(5)	2.35(1)	2.348(5)	2.350(14)
Ln1–O3	2.381(5)	2.37(1)	2.382(5)	2.378(10)
Ln1–O4	2.375(7)	2.34(1)	2.343(5)	2.351(12)
Ln1–O5	2.386(4)	2.351(9)	2.371(5)	2.365(12)
Ln1–O6	2.349(5)	2.307(9)	2.369(4)	2.373(11)
Ln1–O7	2.442(7)	2.41(1)	2.392(5)	2.39(6)
Ln1–O8	2.381(5)	2.35(1)	2.422(5)	2.387(12)
Ln2–O9	2.353(7)	2.35(1)		
Ln2–O10	2.390(5)	2.342(9)		
Ln2–O11	2.373(4)	2.34(1)		
Ln2–O12	2.332(6)	2.33(1)		
Ln2–O13	2.348(7)	2.32(1)		
Ln2–O14	2.359(6)	2.33(1)		
Ln2–O15	2.428(5)	2.37(1)		
Ln2–O16	2.377(5)	2.36(1)		
N1–O1	1.351(7)	1.34(1)		
N3–O9	1.338(9)	1.32(2)		
Ln1–O1–N1	133.4(4)	133.5(8)	135.8(3)	137.9(7)
Ln1–O9–N3	137.7(4)	135(1)		
N1–C1–C2–C7	−2(1)	−2(3)	29.8(9)	−149(1)
N3–C8–C6–C7	36(1)	−35(3)	152.7(6)	153(1)
Ln1–O1–N1–C1	82(1)	−118(1)	72.8(7)	
Ln2–O9–N3–C8	115.1(7)	−84(2)	—	

gelatin capsule. The crystals of **2**, **3** and **5** were first wrapped in polytetrafluoroethylene tape and pressed into a pellet in order to prevent field orientation of the crystals during measurement. Ac measurements were performed with a Quantum Design PPMS using the same samples used for dc measurements. Magnetic data were corrected for diamagnetic contributions of the sample and the sample holder.

2.5 *Ab initio* calculations for compound 3

Ab initio calculations for compound **3** were carried out using the structure obtained from the experimental single-crystal X-ray diffraction analysis. With all other atom positions fixed, the positions of the hydrogen atoms and disordered fluorine atoms were optimized using the program GAUSSIAN 09:[17] Stuttgart/Dresden energy-consistent pseudopotentials (ECP's) and relative double zeta polarized basis sets[18] with the PBE0 functional[19] were employed.

The resulting geometry was used to compute the isotropic magnetic exchange coupling between radical spin units and the Tb^{III} ions, complete active space self-consistent field (CASSCF) calculations were performed without spin–orbit contributions. These were performed with the MOLCAS 8.1 Quantum Chemistry Software Package.[20] The active space consisted of the 7 f-orbitals of the terbium ion and the π^* type radical orbitals (where much of the unpaired electron density of the two radical units are localized) for a total of 10 electrons in 9 active orbitals, *i.e.* CAS(10,9).

Spin orbit coupling effects were then evaluated by computing g-tensor elements of the main magnetic anisotropy axis of Tb^{III} in compound **3**, using the SINGLE_ANISO module in MOLCAS. Table S3 in the ESI† shows the computed energy levels for the Tb^{III} ion obtained from state average restricted active space state interaction (RASSI) calculations with inclusion of spin–orbit coupling, the CASSCF/RASSI-SO method. These energy states were computed by "doping" the organic biradical unit with two extra electrons to make it a dia-

magnetic ligand. Because the organic ligand was rendered closed-shell diamagnetic, the active space became 8 electrons in the 7 f-orbitals of the terbium ion, CAS(8,7). Due to computational resource limitations, only the resultant seven septuplet states were considered and included in the spin orbit calculation.

3 Results and discussion

3.1 Crystal structures

3.1.1 U-shaped dinuclear complexes. Compounds **1** and **2** crystallize in the triclinic $P\bar{1}$ space group, and are isomorphous with only slight differences in the crystal packing. The molecular unit is shown in Fig. 1, and consists of dinuclear species in which each lanthanide(III) ion [Gd (**1**) or Dy (**2**)] has a bicapped trigonal prismatic geometry coordinated by three $hfac^-$ ligands, one IPhIN nitroxide moiety, and one water molecule. Selected bond distances and angles are gathered in Table 2. The Ln–O_{hfac} bond lengths are 2.332(6)–2.442(7)Å (in **1**) and 2.307(9)–2.37(1)Å (in **2**), while the Ln–O_{water} bond lengths are 2.381(5) (Gd1–O8) and 2.377(5)Å (Gd2–O16) for **1**, and 2.35(1) and 2.36(1)Å for Dy1–O8 and Dy2–O16 for **2**. The IPhIN biradical acts as a bridging ligand between two {Ln(hfac)$_3$(H$_2$O)} units. Although IPhIN has two imidazole nitrogen atoms available for coordination, each lanthanide ion is preferentially coordinated by the nitroxide oxygen atoms. The Ln–$O_{nitroxide}$ bond lengths are 2.379(5) and 2.353(7)Å for Gd1–O1 and Gd2–O9 in **1**, and 2.331(9) and 2.35(1) Å for Dy1–O1 and Dy2–O9 in **2**. These bond lengths are in agreement with other gadolinium(III) and dysprosium(III) complexes having lanthanides coordinated by nitroxides.[21,22] The Ln1–O1–N1 and Ln2–O9–N3 bond angles are much closer to each other in **1**, 133.4(4)° and 133.5(8)°, than the analogous bond angles in isomorphous **2**, 137.7(4) and 135(1)°, respectively. One of the biradical conformational torsion angles was almost coplanar with the central *m*-phenylene ring, with ∠N1–C1–C2–C7 −2(1)° in (**1**) and −2(3)° in (**2**), whereas the other ring was significantly twisted with ∠N3–C8–C6–C7 torsion angles of 36(1)° and −35(3)° in **1** and **2**, respectively. Despite this difference, the M–ON coordination sites on the biradical are aligned in the same direction and are *syn* to one another at a fairly close distance. Intramolecular hydrogen bonding between coordinated water molecules and $hfac^-$ moieties is also observed: in compound **2**, the hydrogen bonding for O8 and O16 is bifurcated. These hydrogen bonds probably assist the formation of the molecular U-shaped framework (see Table S1† for geometry parameters), to give the short Ln1···Ln2 distances across the *m*-phenylene unit of 5.7967(8) Å for **1** and 5.778(1) Å for **2**. The intermolecular crystal packing of **1** is further stabilized by C_{sp^2}–H···F interactions, while F···F and C_{sp^3}–H···F short contacts are observed in **2**.

3.1.2 Mononuclear complexes. Complexes **3**, **4** and **5** are also isomorphous, and crystallize in the monoclinic $P2_1/c$ space group. Due to the low quality of crystals of **4** (see Table S2-ESI†), we focus here on the crystal structures of **3** and **5**. These are mononuclear complexes, in which the lanthanide ion (Tb^{III}, **3** or Dy^{III}, **5**) is octacoordinated by three $hfac^-$ ligands, one IPhIN radical and one water molecule, lying in a bicapped trigonal prismatic environment. The Ln–O_{hfac} bond length ranges from 2.343(5) to 2.392(5) Å in **3** and from 2.350(14) to 2.378(10) Å in **5**, while the Ln–O_{water} bond lengths are 2.422(5) (**3**) and 2.387(12) Å (**5**). In contrast to compounds **1** and **2**, the IPhIN biradical acts as a monodentate ligand towards the metal ion for **3** and **5** as shown in Fig. 2. Due to the oxophilic character of the lanthanide ion, the imidazole nitrogen atoms are not coordinated, similar to the situation for **1** and **2**. This coordination mode adopted by the IPhIN bi-

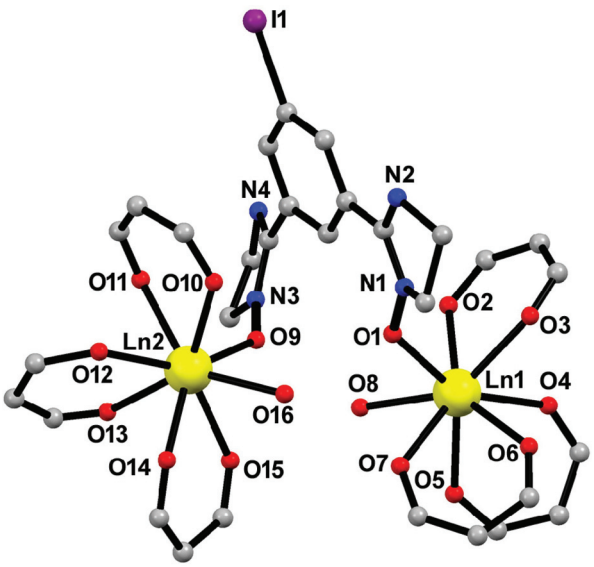

Fig. 1 Molecular structure of compounds **1** (Gd^{III}) and **2** (Dy^{III}). Hydrogen atoms, trifluoromethyl and methyl groups are omitted for the sake of clarity.

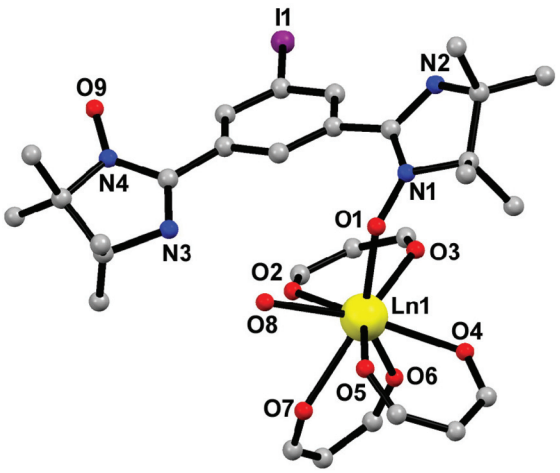

Fig. 2 Molecular structure of compounds **3** (Tb^{III}) and **5** (Dy^{III}). Hydrogen atoms and trifluoromethyl groups are omitted for the sake of clarity.

radical was also previously observed for cobalt(II) and manganese(II) complexes, where only the oxygen atom of the imino nitroxide moiety is coordinated to the metal ions.[4] The Ln–$O_{nitroxide}$ bond lengths are 2.275(4) and 2.270(9) Å, for **4** and **5**, respectively. The Dy–$O_{nitroxide}$ bond length in **5** is slightly shorter than the corresponding bond in **2**. The Tb–$O_{nitroxide}$ bond length in **3** is slightly shorter than that for other terbium(III) compounds coordinated by a nitroxide oxygen atom previously reported in the literature.[10,11,22] The Ln1–O1–N1 bond angle is slightly larger in **5** [137.9(7)°] when compared with that observed in **3** [135.8(3)°]. The torsion angles between the imidazole and phenyl rings are larger than the corresponding angles in **1** and **2**, revealing that monocoordination of the IPhIN biradical allows it to have more structural flexibility compared with dinuclear coordination. The torsion angles between the imidazole and phenyl rings are larger for **3** (∠N1–C1–C2–C3 = 29.8(9)° and ∠N3–C8–C6–C7 = 152.7(6)°) and **5** (∠N1–C1–C2–C3 = −149(1)° and ∠N3–C8–C6–C7 = 153(1)°) than those found for **1–2**.

It is noteworthy that previous work has shown that the torsion angle of radical units relative to a connecting *m*-phenylene ring in similar biradicals can influence magnetic properties, particularly the intramolecular exchange interaction between radical units.[23] This is important, because the IPhIN ligand adopts a coordination mode where each oxygen atom from nitroxide groups is coordinated to (at most) one lanthanide ion. This situation is different from some previously reported lanthanide-based compounds coordinated by bis(nitronyl nitroxides), where oxygen atoms of both the radical units are coordinated to the same ion, adopting a chelating mode.[10,11] The multiple conformational possibilities for coordination in the present case with IPhIN, allows more complexity. For example, the nitroxide moieties (coordinated and uncoordinated) in **3** are oriented in opposite directions, supporting a key structural role for its intramolecular hydrogen bonds involving water ligands and an uncoordinated imidazole nitrogen atom, as shown in Fig. 3. Quite short contacts between the uncoordinated nitroxide oxygen atom (O9) and the neighboring imidazole nitrogen atom ($N2^{i}$, i = $-x,-y,-z$) form at a distance of only 2.926(7) Å for compound **3** in (Fig. 3). But, for these monocoordinate systems, the closest Ln⋯Ln distances are very long, 13.4039(5) Å in **3** and 13.298(1) Å in **5**. The IPhIN *m*-phenylene spacer forms π–π stacks (Fig. 3) with centroid-to-centroid distances and the slip-stacking angles (4.14 Å and 22.5° for **3**, and 4.06 Å and 22.5° for **5**) that are consistent with other reported values for the related structures.[24]

3.2 Magnetic properties

The magnetic properties were investigated in the temperature range 2–290 K for **1–3** and in the temperature ranges 2–240 K and 6.4–300 K for **4** and **5**, respectively. The plots of the product of magnetic molar susceptibility with temperature ($\chi_M T$) *versus* temperature (T) are shown in Fig. 4 and 5 for the dinuclear **1–2** and mononuclear **3–5** complexes, respectively. At high temperature the values of $\chi_M T$ are 16.6, 29.0, 12.5, 8.5 and 14.3 $cm^3\ mol^{-1}\ K$ for compounds **1–5**, respectively: these values are very close to those expected (16.5, 29.1, 12.6, 8.6 and 14.9 $cm^3\ mol^{-1}\ K$) for uncoupled spins. More detailed analyses of the magnetism are given below for the two types of structure.

3.2.1 U-shaped dinuclear complexes 1–2. For compound **1**, $\chi_M T$ remains relatively constant upon cooling, and then increases at lower temperatures, indicating predominant ferromagnetic interactions among the spin carriers. Attempts to reproduce the magnetic data considering only interactions between Gd^{III} ions and isolated radical units were not fruitful, showing the necessity to account for magnetic interactions between spins of the biradical. Therefore, two isotropic exchange interactions were used in a model spin Hamiltonian

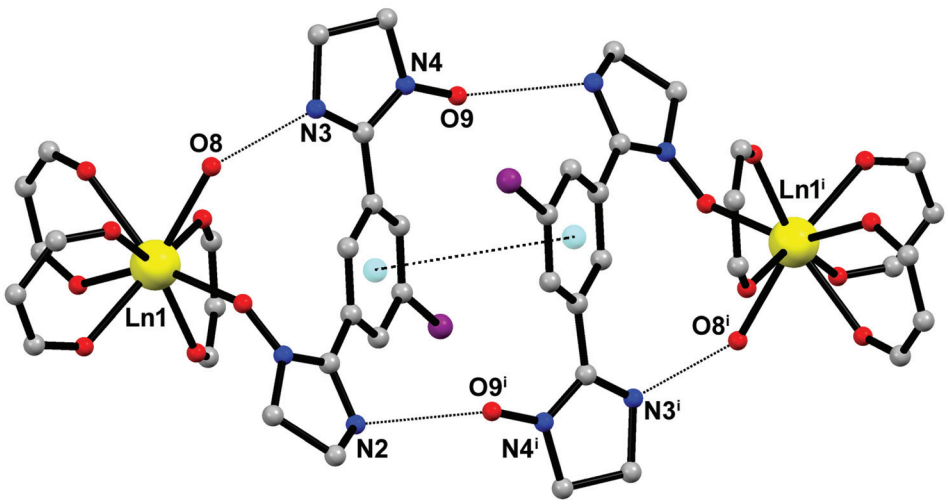

Fig. 3 Details of the crystal packing of compounds **3** and **5**, highlighting the $N_{imidazole}\cdots O_{nitroxide}$ short contacts and π−π stacking between *m*-phenylene rings. Hydrogen atoms, methyl and trifluoromethyl groups are omitted for the sake of clarity.

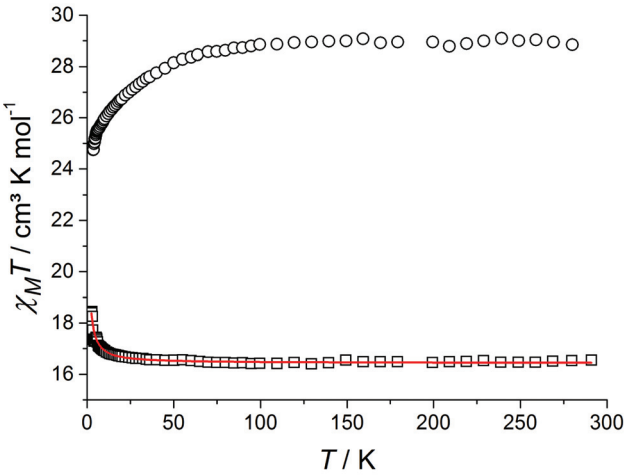

Fig. 4 Thermal dependence of $\chi_M T$ for **1** (□), **2** (○) at $H_{external}$ = 1 kOe. The solid line represents the best fit for **1** using the model of eqn (1).

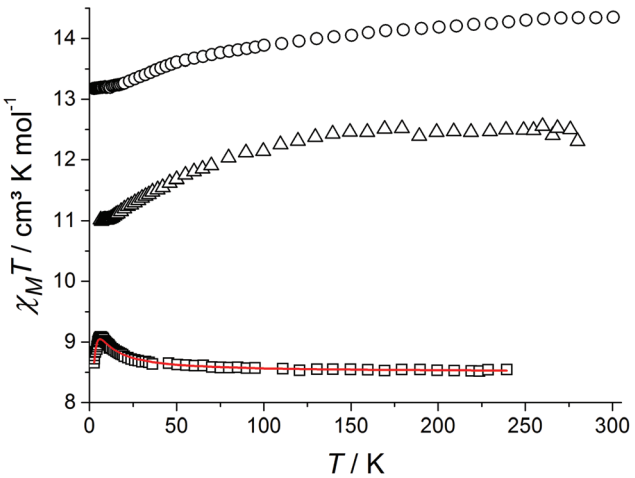

Fig. 5 Thermal dependence of $\chi_M T$ for **3** (△), **4** (□) and **5** (○) at $H_{external}$ = 1 kOe. The solid line represents the best fit for **4** using the model of eqn (2).

(eqn (1)) to consider respectively the interaction between Gd^{III} ions and radicals (J_1), and between the radicals in the biradical unit (J_2). Although the Gd1···Gd2 distance is rather short in the molecular U-shaped framework, this magnetic dipolar interaction should be quite small, and to avoid overparameterization it was not considered.

$$\hat{H} = -J_1(\vec{S}_{Gd1}\cdot\vec{S}_{Rad1} + \vec{S}_{Gd2}\cdot\vec{S}_{Rad2}) - J_2(\vec{S}_{Rad1}\cdot\vec{S}_{Rad2}) + g\mu_B B[\vec{S}_{Rad1} + \vec{S}_{Rad2} + \vec{S}_{Gd1} + \vec{S}_{Gd2}] \quad (1)$$

The magnetic data were fitted using the MagProp routine in the DAVE software suite.[25] The solid line in Fig. 4 shows the best fit parameters found for **1**: g = 1.99 ± 0.01, J_1 = 0.3 ± 0.1 cm^{-1} and J_2 = 6.5 ± 2.7 cm^{-1} with $S_{Gd1} = S_{Gd2}$ = 7/2, and $S_{Rad1} = S_{Rad2}$ = 1/2. The obtained Gd^{III}–$Rad^{\bullet}$ coupling constant J_1 lies within the range observed for the related compounds.[26] Recent magneto-structural studies have found a strong relationship between the Gd^{III}–$Rad^{\bullet}$ exchange coupling and the torsion angle Gd–O–N–C.[27] Ferromagnetic exchange is favored for large torsion angles like those in compound **1**, where Gd1–O1–N1–C1 = 82(1)° and Gd2–O9–N3–C8 = 115.1(7)°. In addition, with respect to exchange between the biradical spins, the dihedral angle between the imidazole ring and the *m*-phenylene unit plays a key role for exchange coupling J_2.[23] For **1**, the inter-ring dihedral angles are not large, which is expected to give ferromagnetic inter-radical exchange coupling J_2, consistent with the fitted result.

For compound **2**, $\chi_M T$ remains constant down to 90 K then decreases at lower temperatures. For compounds containing lanthanide ions other than Gd^{III}, depopulation of the crystal-field split M_J states (Stark sublevels) is especially important in magnetic behavior. Since depopulation of the Stark sublevels occurs simultaneously with possible magnetic exchange interaction and magnetic anisotropy effects, it is very difficult to model the magnetic behavior to quantify Dy–radical and intra-biradical (radical–radical) exchange interactions separately.[28] Nevertheless, since the crystal structure of **2** is quite similar to that of **1**, with comparable torsion angles for Dy–radical interaction, and radical–radical interaction across *m*-phenylene, the nature of the magnetic exchanges is expected to be the same, *i.e.*, both ferromagnetic. Plots of *M vs. H*/*T* data obtained at different temperatures do not superimpose on a single master curve for **2** (Fig. S3 in ESI†). Moreover, the molar magnetization value of 11.9$N\beta$ at 62.5 kOe is low compared to the expected saturation for **2**. Because the expected exchange is ferromagnetic, but the magnetic moment is low, significant magnetic anisotropy and/or low-lying excited states appear to contribute to the magnetism of **2**.

3.2.2 Mononuclear complexes 3–5. For compound **4**, as temperature decreases, $\chi_M T$ increases to a maximum of 9.1 $cm^3\ mol^{-1}$ K at 6.4 K, then decreases to 8.7 $cm^3\ mol^{-1}$ K at 2.6 K, indicating the coexistence of ferro- and antiferromagnetic exchange interactions. These magnetic susceptibility data were fitted using a model spin Hamiltonian (eqn (2)) very similar to the one used for compound **1**, but with only one Gd^{III} ion. The intermolecular magnetic interactions between the molecular units through the O9···N2^{i} short contact are expected to be sufficiently weaker to be ignored in the model; this is also important to prevent overparametrization.

$$\hat{H} = -J_1(\vec{S}_{Gd1}\cdot\vec{S}_{Rad1}) - J_2(\vec{S}_{Rad1}\cdot\vec{S}_{Rad2}) + g\mu_B B[\vec{S}_{Rad1} + \vec{S}_{Rad2} + \vec{S}_{Gd1}] \quad (2)$$

Fitting was performed using the aforementioned software to give the best fit parameters: g = 1.99 ± 0.01, J_1 = 1.4 ± 0.5 cm^{-1} and J_2 = −3.9 ± 0.7 cm^{-1} with S_{Gd1} = 7/2, and S_{Rad1} = 1/2. The metal–radical magnetic coupling constant lies within the range found for other systems having Gd^{III}–radical bonding.[26] However, with respect to the radical–radical inter-

action within the biradical, ferromagnetic interactions are usually found within 1,3-phenylene linked biradicals when the torsion angle between the *m*-phenylene spacer and imidazole rings is less than 60°. A similar ferromagnetic interaction was observed in compound **1** with its modest radical-to-phenylene torsion angle.[23] It is known that metal ions can influence the structural conformation of ligands leading to different intramolecular magnetic interactions between radicals.[10] In our systems, differences between the mononuclear and dinuclear complexes occur with respect to the torsion angles between imidazole and phenyl rings within the biradical unit. Indeed, these two phenylene–radical torsion angles are quite different for the dinuclear compounds (~2° and ~35.5°) but quite similar for the mononuclear ones (~28° and ~30°). Although the dihedral angles in compound **4** are not so large as would be expected to induce antiferromagnetic interaction between radicals in an uncomplexed biradical,[23] still an antiferromagnetic intra-biradical exchange interaction appears to be present in **4** and it does have more total radical to phenylene torsion than in **1**. Possibly there is also some contribution to the overall downturn of the $\chi_M T$ *versus* T plot from antiferromagnetic exchange across the O9···N2^{i} short contacts.

For compounds **3** and **5**, $\chi_M T$ decreases upon cooling temperature down to 11.0 and 13.2 cm^3 mol^{-1} K, respectively. As described for compound **2**, the depopulation of the excited M_J states together with possible magnetic exchange interactions and/or anisotropy precludes separate determination of these magnetic contributions. Nevertheless, since compounds **3** and **5** are isomorphous with **4**, including similar values of the characteristic torsion angles aforementioned, the same nature of magnetic metal–radical and intra-biradical (radical–radical) couplings is expected, *i.e.*, ferromagnetic and antiferromagnetic exchange, respectively. The isothermal field dependencies of the magnetization were measured for **3** at different temperatures and do not superimpose. Therefore, the low molar magnetization values of 6.3$N\beta$ and 6.5$N\beta$ at 62.5 kOe that are observed for compounds **3** and **5**, respectively, indicate significant magnetic anisotropy and/or low-lying excited states (Fig. S4 and S5 in ESI†).

To support the reliability of the experimental exchange couplings, we also performed post-Hartree–Fock *ab initio* calculations to model the behaviour of compound **3**, which was chosen due to its less disordered crystal structure. Indeed, magnetic properties are very sensitive to the structural parameters and, therefore, in the presence of tiny magnetic interactions a reliable geometry is mandatory. The exchange constants J_1 and J_2 (see eqn (2)) were computed from CASSCF energies of the lowest nonuplet, sextuplet, and quartet states of an appropriate biradical–Tb model structure. A ferromagnetic interaction of 0.4 cm^{-1} for the Tb^{III}–radical interaction was computed, with an intra-radical antiferromagnetic interaction of −2.8 cm^{-1}. The value for J_2 fits the behavior of compound **4** (which should not be complicated by spin–orbit coupling), while J_1 is qualitatively correct in being ferromagnetic, but with a predicted magnitude much at variance with the experiment. Clearly the calculation of exchange couplings considering spin–orbit coupling is problematic for ions like Tb^{III}, even qualitatively.[29]

To gain better insight into the magnetic structure of the lanthanide ion in **3**, State Average CASSCF/RASSI-SO computations that include spin–orbit effects were performed. Indeed, although Tb^{III} is a non-Kramer's ion, the ground spin–orbit state and first excited state are quasi-degenerate (see the ESI Table S4†) with an energy gap around 0.3 cm^{-1} and a similar composition in terms of spin-free functions. Therefore these two states form an Ising doublet with a small intrinsic gap.[30] Its magnetic properties were investigated inside the pseudospin framework and its anisotropy axes were calculated using a pseudospin S = 1/2. The main values of the g tensor calculated on the basis of the two lowest states (ESI Table S5†) reveal a pure Ising-type local magnetization on the Tb^{III} ion in agreement with the experimental magnetic data. These are shown pictorially in Fig. 6, along with the predicted magnetic easy axis.

3.2.3 Dynamic magnetic properties of 2. The dynamic properties of compound **2** were investigated by temperature and frequency dependent ac magnetic susceptibility measurements in the range 2.4–15 K at 10 Hz–10 kHz. In the absence of the dc field, the thermal dependences of the in-phase (χ') and out-of-phase (χ'') susceptibilities are shown in Fig. S6 in the ESI† for **2**. The compound clearly exhibits slow relaxation of magnetization, with frequency dependence for both in-phase (χ') and out-of-phase (χ'') susceptibilities: however no maxima were observed down to 2.4 K.

It is well known that for SMMs and SIMs, the fast quantum tunneling of the magnetization (QTM) occurring at resonance fields, mainly in zero field, can be hampered by a nonzero external field. Therefore, the ac susceptibilities were also measured under a static external magnetic field, which shifted the frequency dependence curves to higher temperatures. This behavior is a characteristic signature that QTM is occurring at

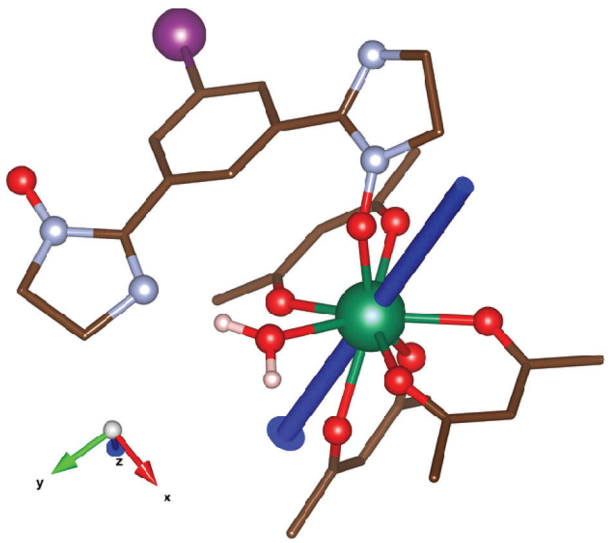

Fig. 6 Orientation of the calculated magnetic easy axis (blue bar) of the ground quasi-doublet of **3**.

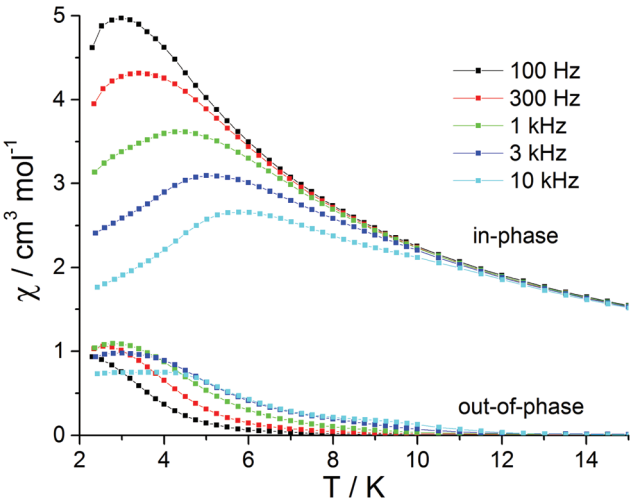

Fig. 7 Thermal dependence of the in-phase and out-of-phase susceptibility components for compound **2** at H = 2 kOe.

zero magnetic field. For an external field H_{ext} = 2 kOe, compound **2** exhibits frequency-dependent maxima for both in-phase and out-of-phase susceptibilities (Fig. 7). The relaxation times obtained from the temperature dependence of the out-of-phase susceptibility maximum were fitted to an Arrhenius law (see the ESI Fig. S7†), to give an energy barrier of $\Delta E/k_B$ = 27 K with a pre-exponential factor $\tau_0 = 1.4 \times 10^{-8}$ s. Furthermore, the value of the relative variation of χ' peak temperature (T_f) per decade frequency (ν) ($K = \Delta T_f/T_f\Delta(\log \nu)$) is 0.24, which is analogous to the behavior seen in superparamagnets and SMMs (0.28).[31]

The shape of the in-phase magnetic susceptibilities at low temperatures, as well as the broad out-of-phase peaks, are consistent with a distribution of relaxation times. Therefore, isothermal ac susceptibility measurements were performed while varying the ac frequency at different temperatures in a fixed external field of 2 kOe (Fig. S8†), and the relaxation distribution width α was calculated by using the Debye formula.[32] At lower temperatures, the distribution broadens drastically, with α increasing from 0.17 at 8 K to 0.57 at 2.4 K. Taken together with the shapes of the in-phase magnetic susceptibilities at low temperature, this large increase of the distribution width suggests more than one relaxation process, which is consistent with the presence of two distinct Dy^{III} ion environments in the crystal structure of compound **2**. Unfortunately, due to the lack of distinctly differentiated peaks in the relaxation data at 2 kOe, any fitting attempt using two relaxation processes results in overparametrization with no reliably independent parameters.

4 Conclusion

We synthesized and characterized two novel families of heterospin complexes containing lanthanide ions and a bis(imino nitroxide) biradical: one with two lanthanide ions coordinated to one biradical moiety, and the other with one lanthanide ion coordinated to the biradical. Ferromagnetic intramolecular magnetic interactions between Gd^{III} and the biradical were found for **1** and **4**, with intramolecular interactions between the radicals being ferro- and antiferromagnetic, respectively. *Ab initio* calculations supported the nature of the magnetic coupling constant obtained experimentally from the Gd^{III} complexes, and predicted the magnetic anisotropy axis elements for Tb^{III} in compound **3**. Compound **2** shows a field dependent slow relaxation of the magnetization consistent with SMM type behavior. Since the nitrogen atoms of IPhIN are not coordinated to any metal ion, **1–5** can be further used as building blocks to synthesize heterometallic compounds, using metal ions that coordinate preferably to nitrogen donor atoms such as first row transition metal ions.

Acknowledgements

Financial support from Brazilian agencies FAPERJ, CAPES, CNPq, and the Science without Borders Program (Special Visiting Researcher – 400808/2012–9) is gratefully acknowledged. We also acknowledge LDRX-UFF (Universidade Federal Fluminense, Brazil), LabCri (Universidade Federal de Minas Gerais, Brazil), Prof. Miguel A. Novak, Prof. Luis Ghivelder from IF-UFRJ and Dr Kleber Pirota (IFGW-UNICAMP) for the use of laboratory facilities. Dr. Federico Totti acknowledges Prof. Roberta Sessoli for the fruitful discussions and European Research Council for funding through the Prof. Sessoli's Advanced Grant MolNanoMaS (no. 267746) and the Computational facilities at the National High-Performance Computing Center in São Paulo (Centro Nacional de Processamento de Alto Desempenho em São Paulo-CENAPAD-SP) for the awarded computational time (proj627).

References

1 D. Luneau and P. Rey, *Coord. Chem. Rev.*, 2005, **249**, 2591; M. G. F. Vaz, R. A. Allão, H. Akpinar, J. A. Schlueter, S. Santos Jr., P. M. Lahti and M. A. Novak, *Inorg. Chem.*, 2012, **51**, 3138; W. Fujita and K. Awaga, *J. Am. Chem. Soc.*, 2001, **123**, 3601; H. Zhao, M. J. Bazile Jr., R. Galań-Mascaros and K. R. Dunbar, *Angew. Chem., Int. Ed.*, 2003, **42**, 1015.

2 A. Caneschi, D. Gatteschi, N. Lalioti, C. Sangregorio, R. Sessoli, G. Venturi, A. Vindigni, A. Rettori, M. G. Pini and M. A. Novak, *Angew. Chem., Int. Ed.*, 2001, **40**, 1760.

3 L. Bogani, A. Vindigni, R. Sessoli and D. Gatteschi, *J. Mater. Chem.*, 2008, **18**, 4750; W.-X. Zhang, R. Ishikawa, B. Breedlove and M. Yamashita, *RSC Adv.*, 2013, **3**, 3772; S. Demira, I.-R. Jeon, J. R. Long and T. D. Harris, *Coord. Chem. Rev.*, 2015, **289–290**, 149; E. Heintze, C. Clauß, M. G. Pini, A. Rettori, F. Totti, M. Dressel and L. Bogani, *Nat. Mater.*, 2013, **12**, 202.

4 M. G. F. Vaz, H. Akpinar, G. P. Guedes, S. Santos Jr., M. A. Novak and P. M. Lahti, *New J. Chem.*, 2013, **37**, 1927.
5 H. L. C. Feltham and S. Brooker, *Coord. Chem. Rev.*, 2014, **276**, 1; D. N. Woodruff, R. E. P. Winpenny and R. A. Layfield, *Chem. Rev.*, 2013, **113**, 5110.
6 L. Bogani and W. Wernsdorfer, *Nat. Mater.*, 2008, **7**, 179; M. N. Leuenberger and D. Loss, *Nature*, 2001, **410**, 789; A. Ardavan, O. Rival, J. J. L. Morton, S. J. Blundell, A. M. Tyryshkin, G. A. Timco and R. E. P. Winpenny, *Phys. Rev. Lett.*, 2007, **98**, 057201; M. A. Novak and R. Sessoli, *Quantum Tunneling of Magnetization QTM 94*, NATO ASI Series 301, Kluwer Academic Press, Dordrecht, The Netherlands, 1995, pp. 171–188.
7 M. G. F. Vaz, R. A. A. Cassaro, H. Akpinar, J. A. Schlueter, P. M. Lahti and M. A. Novak, *Chem. – Eur. J.*, 2014, **20**, 5460; N. Ishii, Y. Okamura, S. Chiba, T. Nogami and T. Ishida, *J. Am. Chem. Soc.*, 2008, **130**, 24; H.-L. Sun, Z.-M. Wang and S. Gao, *Chem. – Eur. J.*, 2009, **15**, 1757; R. A. A. Cassaro, S. G. Reis, T. S. Araujo, P. M. Lahti, M. A. Novak and M. G. F. Vaz, *Inorg. Chem.*, 2015, **54**, 9381.
8 C. R. Ganivet, B. Ballesteros, G. Torre, J. M. Clemente-Juan, E. Coronado and T. Torres, *Chem. – Eur. J.*, 2013, **19**, 1457; N. Ishikawa, M. Sugita, T. Ishikawa, S.-ya. Koshihara and Y. Kaizu, *J. Am. Chem. Soc.*, 2003, **125**, 8694; J. D. Rinehart, M. Fang, W. J. Evans and J. R. Long, *J. Am. Chem. Soc.*, 2011, **133**, 14236.
9 K. Bernot, F. Pointillart, P. Rosa, M. Etienne, R. Sessoli and D. Gatteschi, *Chem. Commun.*, 2010, **46**, 6458.
10 L. Tian, Y.-Q. Sun, B. Na and P. Cheng, *Chem. – Eur. J.*, 2013, 4329.
11 X. Li, T. Li, L. Tian, Z. Y. Liu and X. G. Wang, *RSC Adv.*, 2015, **5**, 74864; S. Y. Zhou, X. Li, T. Li, L. Tian, Z. Y. Liu and X. G. Wang, *RSC Adv.*, 2015, **5**, 17131.
12 K. Bernot, L. Bogani, R. Sessoli and D. Gatteschi, *Inorg. Chim. Acta*, 2007, **360**, 3807.
13 *Bruker. APEX2 v 2014.5-0*, Bruker AXS Inc., Madison, Wisconsin, USA, 2007.
14 *Bruker, SAINT v8.34*, A. Bruker AXS Inc., Madison, Wisconsin, USA, 2013.
15 G. M. Sheldrick, *SADABS, Program for Empirical Absorption Correction of Area Detector Data*, University of Göttingen, Germany, 1996.
16 G. M. Sheldrick, *Acta Crystallogr., Sect. A: Fundam. Crystallogr.*, 2008, **64**, 112.
17 M. J. Frisch, G. W. Trucks, H. B. Schlegel, G. E. Scuseria, M. A. Robb, J. R. Cheeseman, G. Scalmani, V. Barone, B. Mennucci, G. A. Petersson, H. Nakatsuji, M. Caricato, X. Li, H. P. Hratchian, A. F. Izmaylov, J. Bloino, G. Zheng, J. L. Sonnenberg, M. Hada, M. Ehara, K. Toyota, R. Fukuda, J. Hasegawa, M. Ishida, T. Nakajima, Y. Honda, O. Kitao, H. Nakai, T. Vreven, J. A. Montgomery Jr., J. E. Peralta, F. Ogliaro, M. Bearpark, J. J. Heyd, E. Brothers, K. N. Kudin, V. N. Staroverov, R. Kobayashi, J. Normand, K. Raghavachari, A. Rendell, J. C. Burant, S. S. Iyengar, J. Tomasi, M. Cossi, N. Rega, J. M. Millam, M. Klene, J. E. Knox, J. B. Cross, V. Bakken, C. Adamo, J. Jaramillo, R. Gomperts, R. E. Stratmann, O. Yazyev, A. J. Austin, R. Cammi, C. Pomelli, J. W. Ochterski, R. L. Martin, K. Morokuma, V. G. Zakrzewski, G. A. Voth, P. Salvador, J. J. Dannenberg, S. Dapprich, A. D. Daniels, Ö. Farkas, J. B. Foresman, J. V. Ortiz, J. Cioslowski and D. J. Fox, *Gaussian 09, Revision D.01*, Gaussian, Inc., Wallingford, CT, 2009.
18 M. Dolg, H. Stoll, A. Savin and H. Preuss, *Theor. Chem. Acc.*, 1989, **75**, 173.
19 C. Adamo and V. Barone, *J. Chem. Phys.*, 1999, **110**, 6158.
20 F. Aquilante, L. De Vico, N. Ferré, G. Ghigo, P.-Å. Malmqvist, P. Neogrády, T. B. Pedersen, M. Pitonak, M. Reiher, B. O. Roos, L. Serrano-Andrés, M. Urban, V. Veryazov and R. Lindh, *J. Comput. Chem.*, 2010, **31**, 224.
21 L. B. Escobar, G. P. Guedes, S. Soriano, N. L. Speziali, A. K. Jordão, A. C. Cunha, V. F. Ferreira, C. Maxim, M. A. Novak, M. Andruh and M. G. F. Vaz, *Inorg. Chem.*, 2014, **53**, 7508; G. Poneti, K. Bernot, L. Bogani, A. Caneschi, R. Sessoli, W. Wernsdorfer and D. Gatteschi, *Chem. Commun.*, 2007, 1807.
22 H. Tian, R. Liu, X. Wang, P. Yang, Z. Li, L. Li and D. Liao, *Eur. J. Inorg. Chem.*, 2009, 4498.
23 L. Catala, J. Le Moigne, N. Kyritsakas, P. Rey, J. J. Novoa and P. Turek, *Chem. – Eur. J.*, 2001, **7**, 2466.
24 C. Janiak, *J. Chem. Soc., Dalton Trans.*, 2000, 3885.
25 R. T. Azuah, L. R. Kneller, Y. Qiu, P. L. W. Tregenna-Piggott, C. M. Brown, J. R. D. Copley and R. M. Dimeo, *J. Res. Natl. Inst. Stand. Technol.*, 2009, **114**, 341.
26 T. Ishida, R. Murakami, T. Kanetomo and H. Nojiri, *Polyhedron*, 2013, **66**, 183.
27 T. Gupta, T. Rajeshkumar and G. Rajaraman, *Phys. Chem. Chem. Phys.*, 2014, **16**, 14568.
28 J.-P. Sutter and M. L. Kahn, *Magnetism: Molecules to Materials V*, Wiley-VCH, Weinheim, Germany, 2005, p. 161.
29 N. Iwahara and L. F. Chibotaru, *Phys. Rev. B: Condens. Matter*, 2015, **91**, 174438.
30 H. L. C. Feltham, R. Clérac, L. Ungur, V. Vieru, L. F. Chibotaru, A. K. Powell and S. Brooker, *Inorg. Chem.*, 2012, **51**, 10603.
31 M. A. Novak, *J. Magn. Magn. Mater.*, 2004, **272–276**, E707.
32 K. S. Cole and R. H. Cole, *J. Chem. Phys.*, 1941, **9**, 341; M. Costes, J. M. Broto, B. Raquet, H. Rakoto, M. A. Novak, J. P. Sinnecker, S. Soriano, W. S. D. Folly, A. Maignan and V. J. Hardy, *J. Magn. Magn. Mater.*, 2005, **294**, E123.

